Expanded View Figures

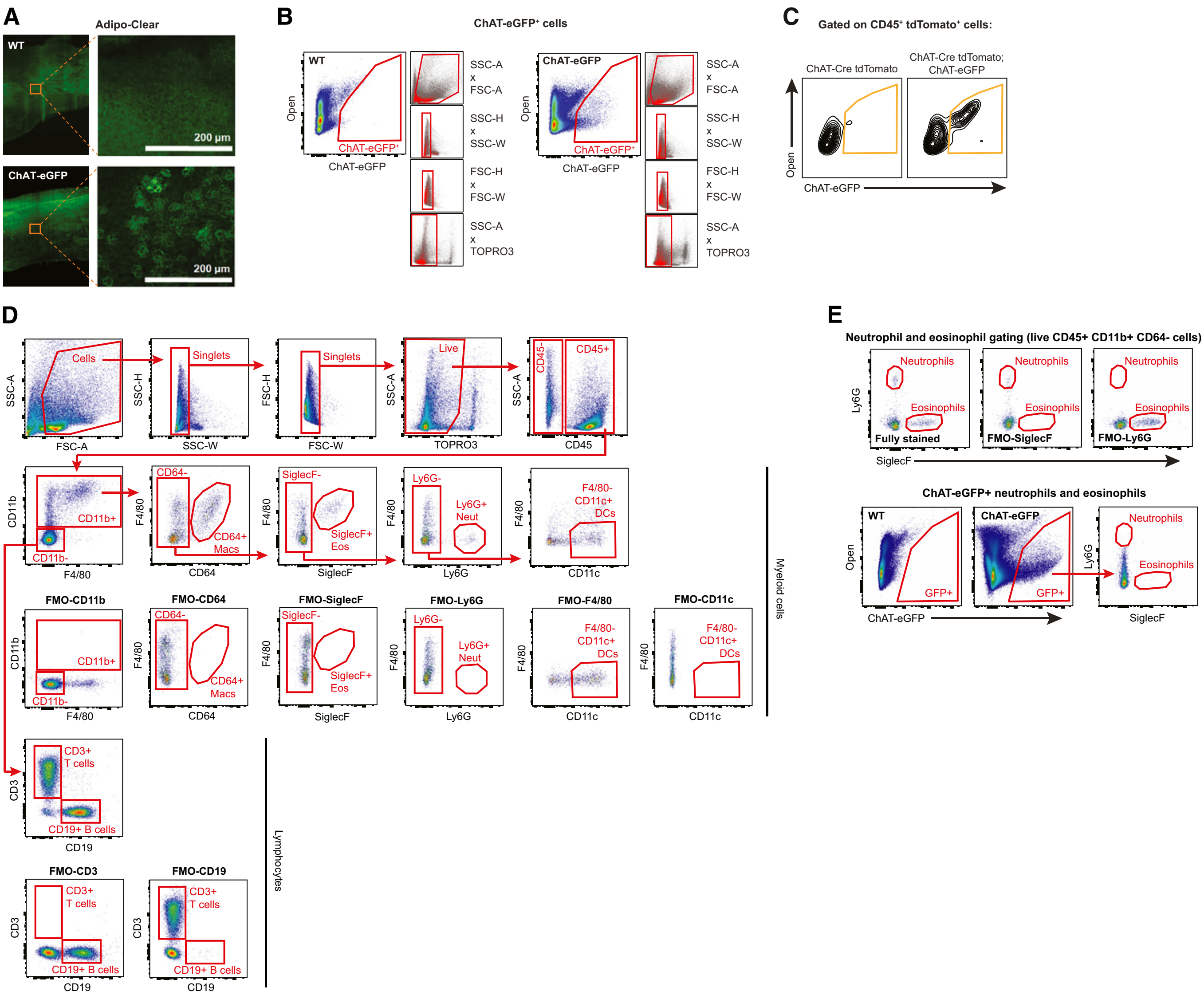

Figure EV1. Related to Fig 1. Acetylcholine-synthesizing macrophages reside in subcutaneous fat.

A High-resolution three-dimensional imaging of WT and ChAT-eGFP IWAT using the Adipo-Clear method (Chi *et al*, 2018) and light-sheet fluorescence microscopy. Whole IWAT was stained with Alexa Fluor 488-conjugated anti-GFP antibody to visualize ChAT-eGFP-expressing cells. High-magnification sections are shown to the right of each sample. Scale bars: 200 µm.

B Representative gating strategy for identification of ChAT-eGFP^{+} cells by flow cytometry. Fluorescence-minus-one (FMO) controls using WT cells were used to define the ChAT-eGFP^{+} population and an open channel (488 nm excitation, 710/50 nm emission) was used to account for autofluorescence. FSC-A, forward scatter area; SSC-A, side-scatter area; SSC-W, side-scatter width; SSC-H, side-scatter height; FSC-H, forward scatter height; FSC-W, forward scatter width.

C Flow cytometric analysis of tdTomato^{+} CD45^{+} ChAT-eGFP^{+} cells in IWAT SVF from *ChAT-Cre*;Ai14 mice (indelible marking of ChAT^{+} cells with tdTomato) or *ChAT-Cre*; Ai14 ChAT-eGFP double reporter mice (GFP marks cells actively expressing ChAT). tdTomato^{+} eGFP^{+} cells are gated orange.

D Representative gating strategy for adipose tissue immunophenotyping. Forward- and side-scatter properties were used to remove debris and doublets, and a viability dye was used to exclude dead cells. FMOs were included to demarcate the positive and negative populations for each molecular surface marker. Within the hematopoietic (CD45^{+}) population, the following cell types were defined: MΦ (Macs; CD11b^{+} CD64^{+}), eosinophils (Eos; CD11b^{+} CD64^{-} SiglecF^{+}), neutrophils (Neut; CD11b^{+} CD64^{-} SiglecF^{-} Ly6G^{+}), dendritic cells (DCs; CD11b^{+} CD64^{-} SiglecF^{-} Ly6G^{-} F4/80^{-} CD11c^{+}), T cells (CD11b^{-} CD3^{+} CD19^{-}), and B cells (CD11b^{-} CD3^{-} CD19^{+}).

E Top: Representative gating strategy for identification of neutrophils and eosinophils in IWAT, using FMOs to define gate boundaries. Bottom: Absence of ChAT-eGFP^{+} neutrophils and eosinophils in IWAT.

Figure EV2. Related to Fig 1. Acetylcholine-synthesizing macrophages reside in subcutaneous fat.

A Percentages of $CD45^+$ and $CD45^-$ cells labeled RFP^- or RFP^+ by flow cytometric analysis of ChAT-eGFP;*Vav-iCre*-RFP IWAT (n = 6). To confirm the hematopoietic specificity and efficiency of the *Vav-iCre* driver, we generated ChAT-eGFP;*Vav-iCre*-RFP mice in which RFP expression was under the control of a *loxP*-flanked STOP cassette. *Vav-iCre* was highly specific for $CD45^+$ hematopoietic cells (compared with $CD45^-$ cells), and shown very high efficiency for recombination in immune cell types such as T cells, B cells, and MΦ.

B Percentages of T cells, B cells, and MΦ labeled RFP^- or RFP^+ by flow cytometric analysis of ChAT-eGFP;*Vav-iCre*-RFP IWAT (n = 6).

C Percentage of total ChAT-$eGFP^+$ cells labeled RFP^- or RFP^+ by flow cytometric analysis of ChAT-eGFP;*Vav-iCre*-RFP IWAT (n = 6). Double positivity for ChAT-eGFP and *Vav-iCre-RFP*, confirmed *Vav-iCre* as a relevant hematopoietic deletion model to study ChAT-expressing immune cells.

D Percentages of ChAT-$eGFP^+$ T cells, B cells and MΦ labeled RFP^- or RFP^+ by flow cytometric analysis of ChAT-eGFP;*Vav-iCre*-RFP IWAT (n = 6).

E Representative flow plots showing the percentage of ChAT-$eGFP^+$ MΦ (out of all IWAT MΦ) at RT and after 4 h CE. Related to Fig 1H.

F Left: T cells as a percentage of all ChAT-$eGFP^+$ cells at RT and CE (n = 11). Right: Total number of ChAT-$eGFP^+$ T cells at RT and CE (n = 11).

G Left: B cells as a percentage of all ChAT-$eGFP^+$ cells at RT and CE (n = 11). Right: Total number of ChAT-$eGFP^+$ B cells at RT and CE (n = 11).

H Other $CD45^+$ cells as a percentage of all ChAT-$eGFP^+$ cells at RT and CE (n = 11).

I Ki67 expression in IWAT MΦ from mice fed a chow diet or high-fat diet (HFD), included as a positive control, since increasing expression of Ki67 has previously been reported for adipose MΦ from mice fed a high-fat diet compared with chow (Amano *et al*, 2014). Counts are normalized to the mode.

J Relative mRNA levels (pseudocounts) of genes relevant to acetylcholine signaling, including the choline transporter (*Slc5a7*) and the vesicular acetylcholine transport (*Slc18a3*), in ChAT-$eGFP^-$ (n = 4) and ChAT-$eGFP^+$ (n = 3) MΦ by RNA-seq. Related to Fig 1L.

K Relative mRNA levels of *Chat*, *Slc18a3*, and *Slc5a7* in sorted ChAT-$eGFP^-$ and ChAT-$eGFP^+$ hematopoietic cells ($CD45^+$) (n = 4). Gene expression was analyzed by qPCR and normalized to levels of *Tbp* using the $2^{-\Delta\Delta Ct}$ method.

L Relative *Chat* expression in sorted T cells ($CD45^+$ $CD11b^-$ $CD3^+$ $CD19^-$), B cells ($CD45^+$ $CD11b^-$ $CD3^-$ $CD19^+$), and MΦ ($CD45^+$ $CD11b^+$ $CD64^+$) from WT IWAT (n = 4). Gene expression was analyzed by qPCR and normalized to levels of *Tbp* using the $2^{-\Delta\Delta Ct}$ method.

M, N RNA-seq data for fat-derived $Lyve1^{hi}$ and $Lyve1^{lo}$ MΦ (Chakarov *et al*, 2019) were procured from the Gene Expression Omnibus (GEO) Series Accession GSE125667. (M) Biological pathway analysis of enriched genes in $Lyve1^{lo}$, $Lyve1^{hi}$ (left), or ChAT-$eGFP^+$ MΦ (right) was performed. Common biological pathways were not detected across the subpopulations. $Lyve1^{lo}$ and $Lyve1^{hi}$ MΦ highly expressed genes for immune regulation and/or inflammation, whereas ChAT-$eGFP^+$ MΦ revealed enriched expression of genes in neuronal and adrenergic signaling. (N) Relative expression (pseudocounts) of genes relevant to acetylcholine signaling in $Lyve1^{hi}$, $Lyve1^{lo}$, and ChAT-$eGFP^+$ MΦ (n = 3). Counts for *Gfp*, *Chat*, *Bche*, and *Slc18a3* were not available in the GSE125667 dataset.

O–R RNA-seq data for subcutaneous fat-derived sympathetic neuron-associated MΦ (SAM) (Pirzgalska *et al*, 2017) were procured from the GEO Series Accession GSE103847. (O) Biological pathway analysis of commonly enriched genes in SAM and ChAT-$eGFP^+$ MΦ. (P) Gene expression correlation plot between ChAT-$eGFP^+$ MΦ and SAM. Spearman's correlation coefficient (r) test did not indicate strong association in global gene expression between ChAT-$eGFP^+$ MΦ and SAM. (Q) Biological pathway analysis of uniquely expressed genes in ChAT-$eGFP^+$ MΦ versus SAM. Transcriptomic comparison of ChAT-$eGFP^+$ MΦ and SAM suggested overlapping molecular features in intrinsic macrophage marker profiles or properties. However, ChAT-$eGFP^+$ MΦ was identified as a distinct population from SAM with an enrichment of neuronal signaling. (R) Relative expression (pseudocounts) of genes relevant to acetylcholine signaling in ChAT-$eGFP^+$ MΦ and SAM (n = 3 for ChAT-$eGFP^+$ MΦ, 2 for SAM). Counts for *Gfp* were not available in the GSE103847 dataset.

Data information: In (A–D, F–H and J–K), data are presented as mean ± SEM where *$P < 0.05$, **$P < 0.01$, and ***$P < 0.001$ (two-tailed Student's t-test). In (L), data are presented as mean ± SEM and the letters "a" and "b" indicate $P < 0.05$ between groups (one-way ANOVA).

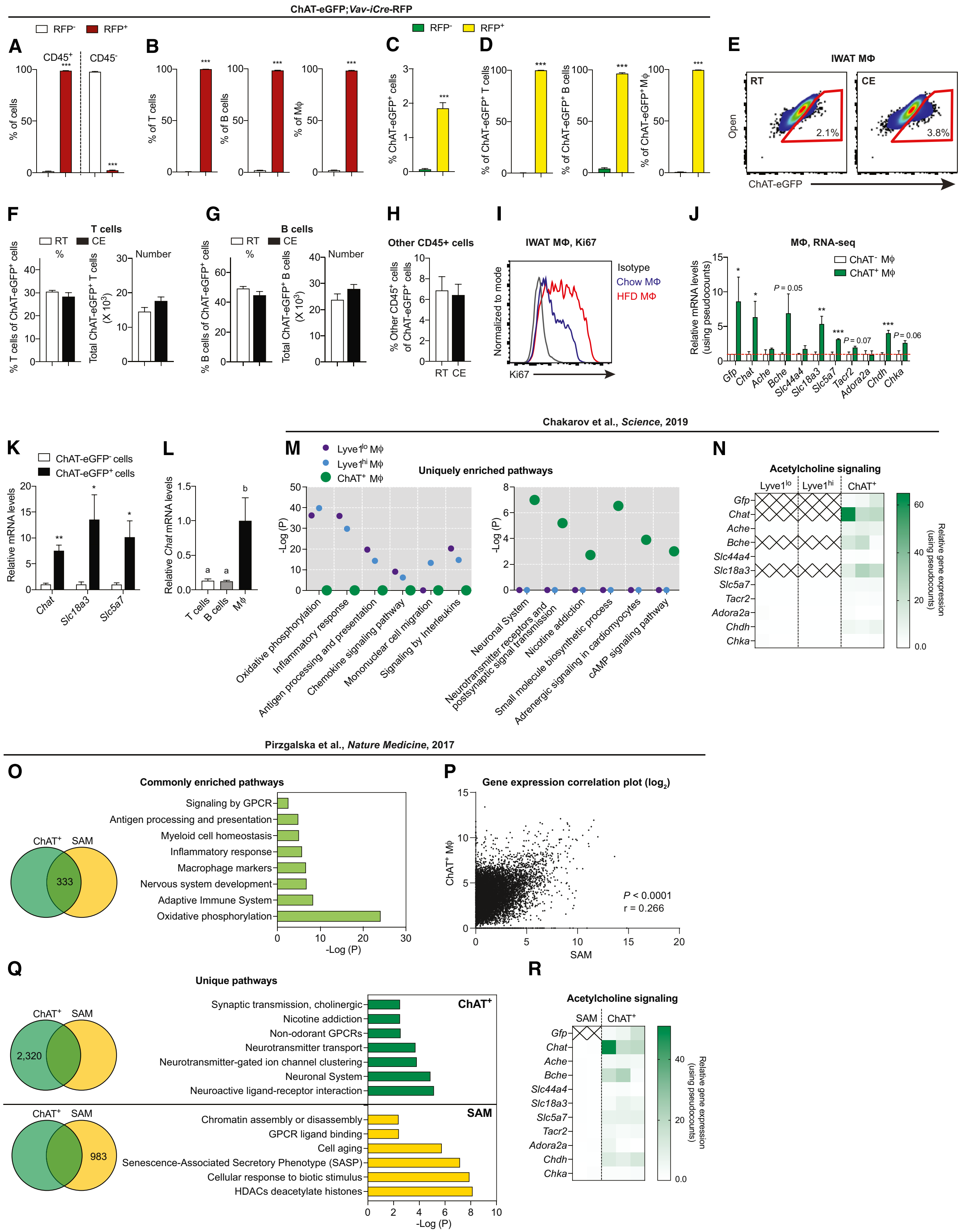
ChAT-eGFP;Vav-iCre-RFP
A
B
C
D
E
IWAT MΦ
RT
CE
2.1%
3.8%
ChAT-eGFP
F
T cells
G
B cells
H
Other CD45+ cells
I
IWAT MΦ, Ki67
Isotype
Chow MΦ
HFD MΦ
J
MΦ, RNA-seq
Chakarov et al., Science, 2019
K
L
M
Uniquely enriched pathways
N
Acetylcholine signaling
Pirzgalska et al., Nature Medicine, 2017
O
Commonly enriched pathways
P
Gene expression correlation plot (log2)
Q
Unique pathways
R
Acetylcholine signaling

Figure EV2.

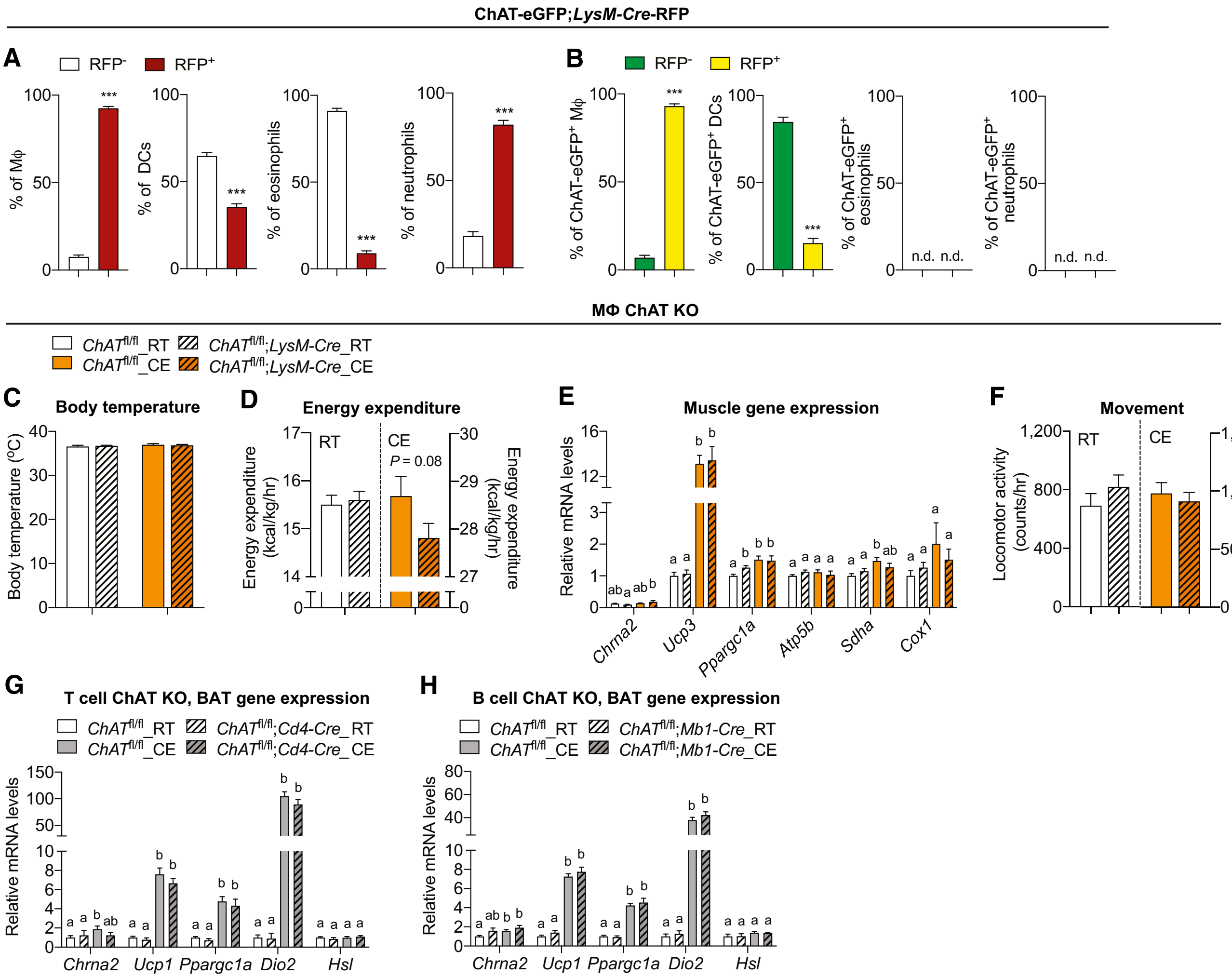

Figure EV3. Related to Fig 2. Loss of ChAT in macrophages compromises the adaptive thermogenic capacity of subcutaneous fat.

A Percentages of MΦ, DCs, eosinophils and neutrophils labeled RFP$^-$ or RFP$^+$ by flow cytometric analysis of ChAT-eGFP;*LysM-Cre*-RFP IWAT showing specificity and efficiency of *LysM-Cre*-driven recombination in myeloid cell types (n = 5). Variations in specificity and efficiency of the *LysM-Cre* driver in different tissue settings have been reported since its inception (Clausen *et al*, 1999), where it deletes to varying extents among myeloid cell types including MΦ, granulocytes, and DCs (Abram *et al*, 2014; Shi *et al*, 2018). As such, we generated ChAT-eGFP;*LysM-Cre*-RFP mice to assess *LysM-Cre*-driven labeling in IWAT myeloid cells, and in particular, in our ChAT-expressing cells of interest. MΦ exhibited the highest degree of RFP$^+$ labeling, at > 90%, while neutrophils (~80%), DCs (~35%), and eosinophils (~9%) were also labeled RFP$^+$ to lesser extents.

B Percentages of ChAT-eGFP$^+$ MΦ, DCs, eosinophils, and neutrophils labeled RFP$^-$ or RFP$^+$ by flow cytometric analysis of ChAT-eGFP;*LysM-Cre*-RFP IWAT (n = 5). ChAT-eGFP$^+$ eosinophils and neutrophils were not detected (n.d.). > 90% of ChAT-eGFP$^+$ MΦ were RFP$^+$, confirming the utility of the *LysM-Cre* model in studying ChAT-expressing MΦ. In contrast, the proportionally minor ChAT-eGFP$^+$ DC population exhibited only ~15% RFP$^+$ labeling, while no ChAT-eGFP$^+$ eosinophils or neutrophils were detected.

C Rectal core body temperature of *ChAT*$^{fl/fl}$ and *ChAT*$^{fl/fl}$;*LysM-Cre* mice housed at RT (n = 10 for *ChAT*$^{fl/fl}$, n = 14 for *Cre*) or 6 h CE (n = 9 for *ChAT*$^{fl/fl}$, n = 13 for *Cre*).

D Average energy expenditure of *ChAT*$^{fl/fl}$ (n = 10) and *ChAT*$^{fl/fl}$;*LysM-Cre* (n = 14) mice housed in metabolic chambers at RT or CE for 6 h (from 9 a.m. to 3 p.m.).

E Relative mRNA expression of *Chrna2* and shivering thermogenic genes in skeletal muscle of *ChAT*$^{fl/fl}$ and *ChAT*$^{fl/fl}$;*LysM-Cre* mice housed at RT (n = 10) or 6 h CE (n = 8). Gene expression was analyzed by qPCR and normalized to levels of *Tbp* using the $2^{-\Delta\Delta Ct}$ method.

F Average locomotor activity of *ChAT*$^{fl/fl}$ (n = 10) and *ChAT*$^{fl/fl}$;*LysM-Cre* (n = 14) mice housed in metabolic chambers at RT or CE for 6 h (from 9 a.m. to 3 p.m.).

G, H Relative mRNA expression of *Chrna2* and thermogenic genes in BAT of *ChAT*$^{fl/fl}$;*Cd4-Cre* (n = 14 for *ChAT*$^{fl/fl}$_RT, n = 8 for *Cre*_RT, n = 16 for *ChAT*$^{fl/fl}$_CE, n = 9 for *Cre*_CE) (G), *ChAT*$^{fl/fl}$;*Mb1-Cre* (n = 9 for *ChAT*$^{fl/fl}$_RT, n = 10 for *Cre*_RT, n = 9 for *ChAT*$^{fl/fl}$_CE, n = 9 for *Cre*_CE) (H) and littermate *ChAT*$^{fl/fl}$ mice housed at RT or 6 h CE.

Data information: In (A–D and F), data are presented as mean ± SEM where ***P < 0.001 (two-tailed Student's t-test). In (E and G–H), data are presented as mean ± SEM and the letters "a" and "b" indicate P < 0.05 between groups (one-way ANOVA).

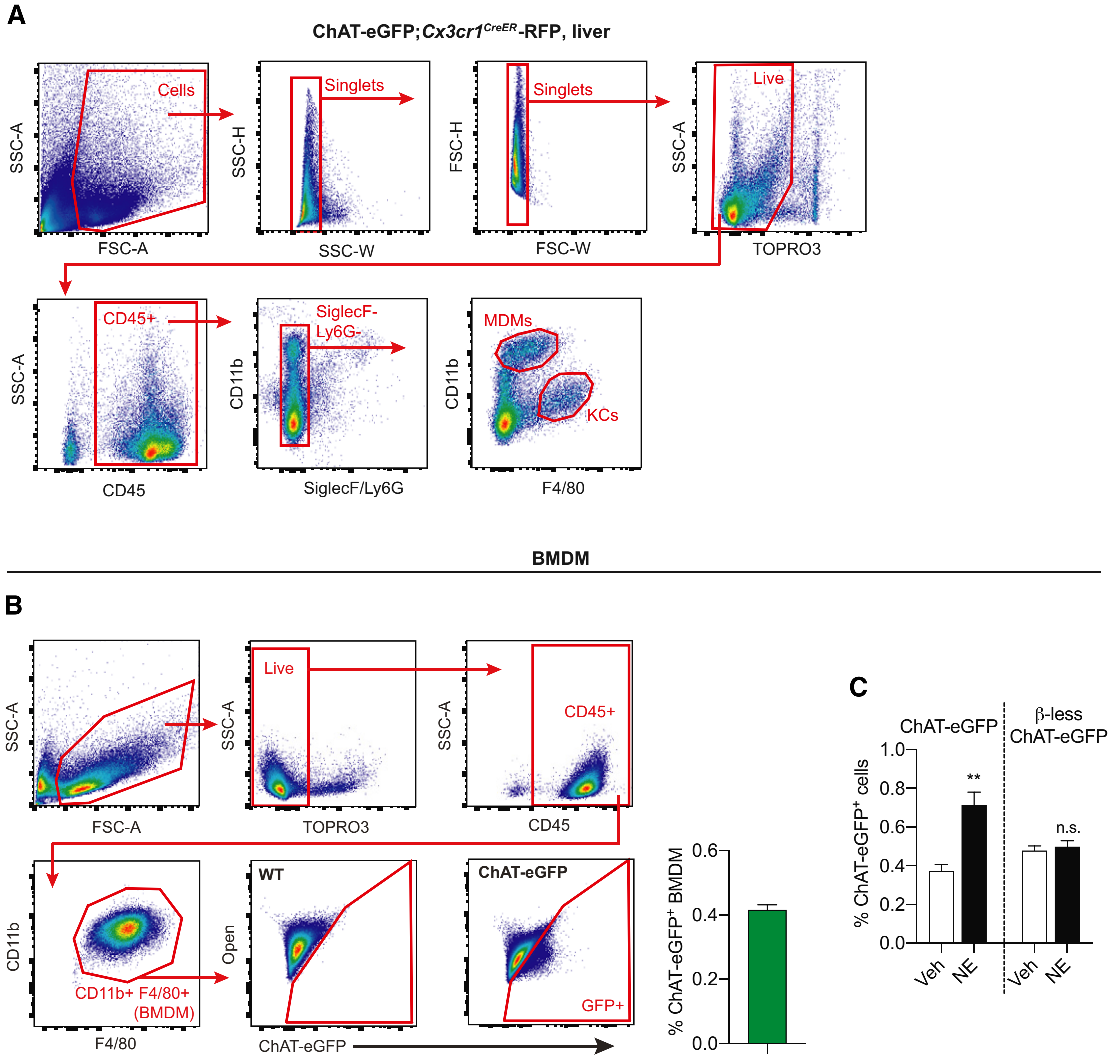

Figure EV4. Related to Fig 3. ChAMs link adrenergic signaling to beige fat activation.

A Representative gating strategy for identification of monocyte-derived MΦ (MDMs; $CD45^+$ $SiglecF^-$ $Ly6G^-$ $CD11b^{hi}$ $F4/80^{lo}$) and Kupffer cells (KCs; $CD45^+$ $SiglecF^-$ $Ly6G^-$ $CD11b^{lo}$ $F4/80^{hi}$) in liver non-parenchymal cells.

B Left: Representative gating strategy for identification of BMDMs ($CD45^+$ $CD11b^+$ $F4/80^+$). WT BMDMs were used as an FMO control to establish the ChAT-$eGFP^+$ gate. Right: Percentage of BMDMs that were ChAT-$eGFP^+$ (n = 24).

C Percentage of BMDMs grown from ChAT-eGFP and β-less ChAT-eGFP mice that are ChAT-$eGFP^+$ following 2-h treatment with veh or 100 μM NE (n = 4). Data were drawn from the same experiments as Fig 3M. n.s.: not significant.

Data information: In (B-C), data are presented as mean ± SEM where $***P < 0.001$ (two-tailed Student's t-test).

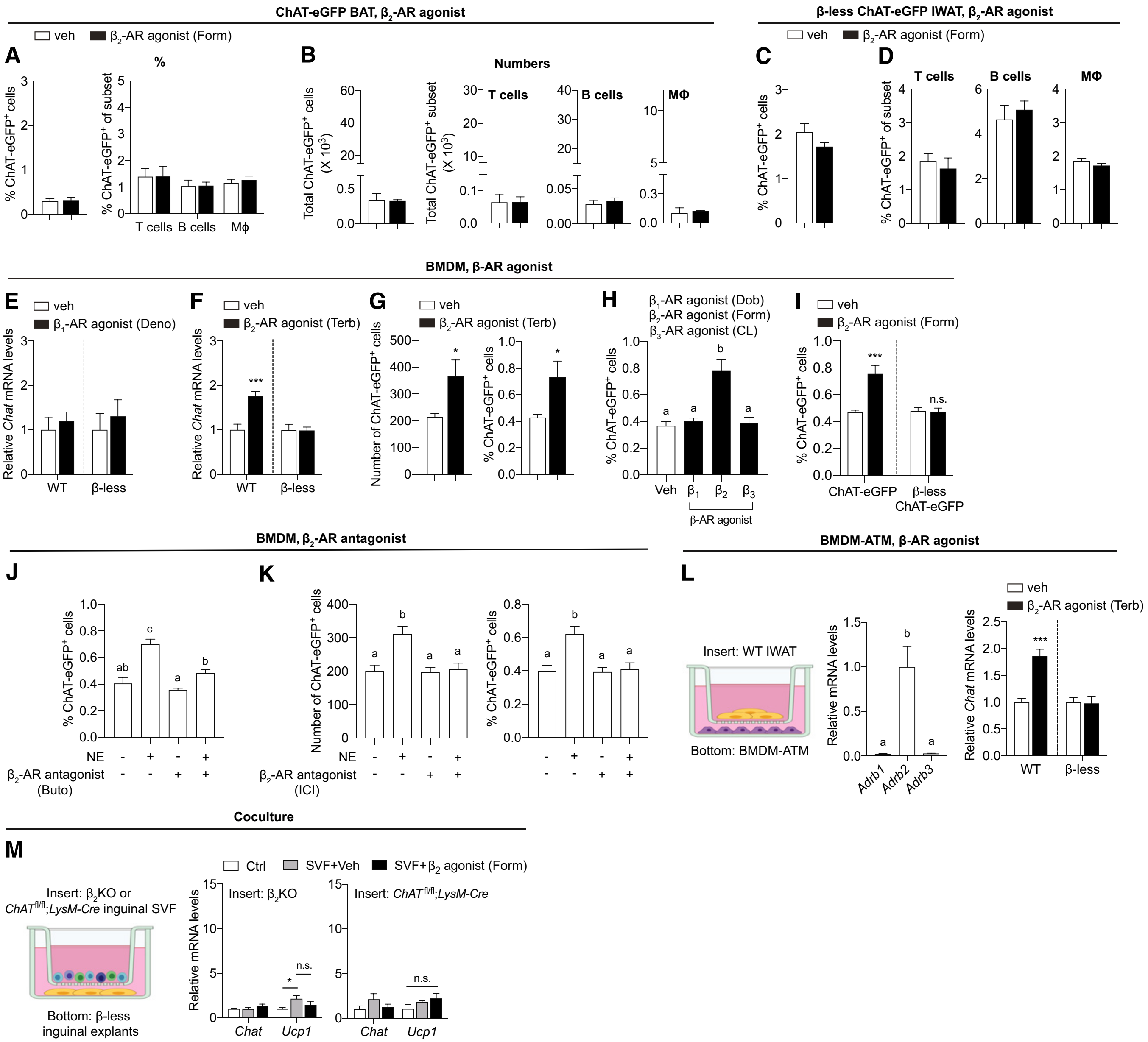

ChAT-eGFP BAT, β2-AR agonist
β-less ChAT-eGFP IWAT, β2-AR agonist
veh
β2-AR agonist (Form)
A
B
C
D
%
Numbers
T cells
B cells
MΦ
BMDM, β-AR agonist
E
F
G
H
I
β1-AR agonist (Deno)
β2-AR agonist (Terb)
β1-AR agonist (Dob)
β2-AR agonist (Form)
β3-AR agonist (CL)
Relative Chat mRNA levels
WT
β-less
ChAT-eGFP
β-less ChAT-eGFP
β-AR agonist
BMDM, β2-AR antagonist
BMDM-ATM, β-AR agonist
J
K
L
NE
β2-AR antagonist (Buto)
β2-AR antagonist (ICI)
Insert: WT IWAT
Bottom: BMDM-ATM
Adrb1
Adrb2
Adrb3
Coculture
M
Insert: β2KO or ChAT fl/fl;LysM-Cre inguinal SVF
Bottom: β-less inguinal explants
Ctrl
SVF+Veh
SVF+β2 agonist (Form)
Insert: β2KO
Insert: ChAT fl/fl;LysM-Cre
Chat
Ucp1

Figure EV5.

Figure EV5. Related to Fig 4. ChAMs function via activation of the β_2-AR.

A, B ChAT-eGFP mice were treated for 4 h with veh or β_2-AR agonist (1 mg/kg formoterol, Form), and the (A) percentage of total BAT SVF cells (left) and of total T cells, B cells, and MΦ (right) that were ChAT-eGFP$^+$ were measured by flow cytometry, in addition to (B) the total number of ChAT-eGFP$^+$ cells (left), ChAT-eGFP$^+$ T cells, B cells, and MΦ (right) (n = 3).

C, D β-less ChAT-eGFP mice were treated for 4 h with veh or β_2-AR agonist (1 mg/kg Form) and the percentage of (C) ChAT-eGFP$^+$ IWAT SVF cells and (D) ChAT-eGFP$^+$ T cells, B cells, and MΦ was measured by flow cytometry (n = 4).

E, F BMDMs were isolated and grown from WT and β-less mice, then treated for 2 h with (E) veh or β_1-AR agonist (2.5 μM denopamine, Deno) (n = 6) or (F) veh or β_2-AR agonist (10 μM terbutaline, Terb) (n = 4). *Chat* mRNA expression was measured by qPCR and normalized to levels of *Tbp* using the $2^{-\Delta\Delta Ct}$ method.

G Total number of ChAT-eGFP$^+$ cells (left) and percentage of ChAT-eGFP$^+$ cells (right) in BMDMs treated for 2 h with veh or β_2-AR agonist (10 μM Terb) (n = 4). An equal number of events (50,000) were analyzed by flow cytometry.

H Percentage ChAT-eGFP$^+$ cells of all BMDMs derived from ChAT-eGFP mice. BMDMs were treated for 2 h with veh or β_1-AR agonist (2.5 μM Dob), β_2-AR agonist (2.5 μM Form) or β_3-AR agonist (2.5 μM CL); then, an equal number of events (50,000) were analyzed by flow cytometry (n = 4). Data were drawn from the same experiments as Fig 4J.

I Percentage of ChAT-eGFP$^+$ cells of all BMDMs derived from ChAT-eGFP and β-less ChAT-eGFP mice. BMDMs were treated for 2 h with veh or β_2-AR agonist (2.5 μM Form); then, an equal number of events (50,000) were analyzed by flow cytometry (n = 4). Data were drawn from the same experiments as Fig 4K. n.s: not significant.

J Percentage of ChAT-eGFP$^+$ cells, of all BMDMs. ChAT-eGFP BMDMs were treated for 2 h with veh or pan β-AR agonist (100 μM NE), β_2-AR antagonist (5 μM butoxamine, Buto) or a combination of NE and β_2-AR antagonist (Buto). An equal number of events (50,000) were analyzed by flow cytometry (n = 4). Data were drawn from the same experiments as Fig 4M.

K BMDMs were treated for 2 h with veh or pan β-AR agonist (100 μM NE), β_2-AR antagonist (5 μM ICI 118,551, ICI), or a combination of NE and β_2-AR antagonist (ICI) (n = 8). Total number of ChAT-eGFP$^+$ BMDMs (left) and the percentage of ChAT-eGFP$^+$ cells of all BMDMs (right) were measured. An equal number of events (50,000) were analyzed by flow cytometry.

L Left: Schematic showing bicompartmental co-culture system for growing BM-ATMs, whereby BMDMs are differentiated, then grown for 2 days in the presence of IWAT in the upper chamber. Middle: Relative mRNA expression of *Adrb1*, *Adrb2,* and *Adrb3* in BM-ATMs (n = 6). mRNA expression was measured by qPCR and normalized to levels of *Tbp* using the $2^{-\Delta\Delta Ct}$ method. Right: Relative *Chat* mRNA expression in BM-ATMs isolated and differentiated from WT or β-less mice, treated for 2 h with vehicle or β_2-AR agonist (10 μM Terb) (n = 4). mRNA expression was measured by qPCR and normalized to levels of *Tbp* using the $2^{-\Delta\Delta Ct}$ method.

M Left: Bicompartmental co-culture system with media alone (Ctrl) or SVF cells isolated from β_2KO or *ChAT*$^{fl/fl}$;*LysM-Cre* IWAT in the upper compartment (transwell insert) and freshly isolated IWAT explants from β-less mice in the lower compartment. Cells were co-cultured for 4h in the presence or absence of 2.5 μM β_2-AR agonist (Form). 150 μM rivastigmine was added to the media to prevent degradation of Ach. Right: qPCR analyses of *Chat* and *Ucp1* mRNA levels in β-less explants following co-culture with media, vehicle- or β_2-AR agonist-treated SVF cells from β_2KO (n = 4) or *ChAT*$^{fl/fl}$;*LysM-Cre* (n = 3) IWAT. mRNA expression was measured by qPCR and normalized to levels of *Tbp* using the $2^{-\Delta\Delta Ct}$ method. n.s.: not significant.

Data information: In (A–G, I and L–M), data are presented as mean ± SEM where *P < 0.05 and ***P < 0.001 (two-tailed Student's t-test). In (H and J–L), data are presented as mean ± SEM and the letters "a", "b" and "c" indicate P < 0.05 between groups (one-way ANOVA).

